Noise and Signal modeling of various VCSEL structures.

Angelique Rissons[a*], Julien Perchoux[a*], Jean-Claude Mollier[a*], Martin Grabherr[b**]
[a] Supaero/MOSE group, 10 Avenue Edouard Belin, BP 4032, 31055 Toulouse CEDEX4, France
[b] U-L-M Photonics GmbH, Albert-Einstein-Allee 45, D89081 Ulm/Germany

ABSTRACT

Current evolution in Datacoms and Gigabit Ethernet have made 850nm Vertical Cavity Surface Emitting Lasers (VCSEL) the most important and promising emitter. Numerous different structures have been growth, to obtain best current confinement and then to control the emitted light modal behavior. We have developed a small signal equivalent electrical model of VCSEL including Bragg reflectors, active area, chip connection and noise behavior. Easy to integrate with classical software for circuit studies, this model which is widely adaptable for different structures takes into account the complete electrical environment of the chip. An experimental validation for RF modulation up to 10 GHz has been realized on oxide confined VCSEL, demonstrating that the model could be used to get realistic values for the VCSEL intrinsic parameters.
Including Langevin noise sources into the rate equations and using the same electrical analogy, noise current and voltage sources can be added to the model. It allows good prediction for the RIN function shape up to 10GHz for monomodal emitter.

Keywords: VCSEL, Oxide aperture, RIN, Electrical Modeling, Rate Equations

1. INTRODUCTION

The rise of multi-channel optical transmissions supports the development of the VCSEL (Vertical-Cavity Surface-Emitting Laser). Indeed, the properties of this laser diode allow to design small size optical modules for Gigabit Ethernet applications. The good performances and the maturity of the AlGaAs/GaAs technology are the bases of a VCSEL widely used in short haul links at 850nm. All VCSEL applications need a perfect knowledge of the electrical behavior which can be described by a model usable at the same time by the manufacturer and the user.
Therefore, the electrical and optical phenomena are represented by a small signal equivalent circuit [1]. This modeling is based on the rate equations of carrier and photon numbers which are determined by including the VCSEL specificities (Quantum Wells and Distributed Bragg Reflectors) and the contribution of the Langevin noise sources related to the electron and photon fluctuations. By injecting on the component a small signal modulation, the rate equations has been linearized to be connected with the equivalent circuit equations of the VCSEL cavity giving relations between the intrinsic parameters and the circuit elements. Including the noise sources in the electrical equivalent circuit of the VCSEL cavity, relationships between the spectral densities of the noise sources and the intrinsic parameters were obtained as well.
The validation of that model was achieved from the measurement of the electrical reflection and transmission coefficient on Ulm Photonics oxide confined VCSELs. A study of different aperture sizes and an optimization of the circuit elements allow to extract values of the intrinsic parameters.
Another experimental investigation aims at measuring the Relative Intensity Noise (RIN) of each VCSEL aperture size and optimizing the noise sources amplitude by using the intrinsic parameters values.

2. RATE EQUATIONS AND SMALL SIGNAL EQUIVALENT CIRCUIT OF DIFFERENT VCSEL STRUCTURES

2.1. VCSEL rate equations

This model is based on VCSEL rate equations, including the Distributed Bragg Reflectors (DBR) contribution and the vertical light emission. Although the VCSEL features a multimode-transverse behavior, that paper is restricted to the important case of monomode transverse [2]. The rate equation can then be written in the following form :

$$\frac{dN}{dt} = \frac{\eta_i \cdot I}{q \cdot N_w} - (A + B \cdot N) \cdot N - G \cdot P + F_N(t) \quad (1)$$

$$\frac{dP}{dt} = N_w \cdot \Gamma \cdot \beta \cdot B \cdot N^2 + N_w \cdot G \cdot P - \frac{P}{\tau_p} + F_p(t) \quad (2)$$

where the carrier number (N) rate equations is considered in one Quantum Well (QW) while the photon number (P) rate equation takes into account the whole cavity. N_w is the QW number. $\frac{\eta_i \cdot I}{q \cdot N_w}$ represents the current injected in each QW with I the bias current and q the electron charge.

A and B are the non-radiative and the bimolecular recombination coefficients (for 850nm VCSELs, the Auger recombination can be neglected).

G is the modal gain such as:

$$G = g_0 \cdot \frac{N - N_{tr}}{1 + \varepsilon \cdot P} \quad (3)$$

and $g_o = v_{gr} \cdot \Gamma \cdot \frac{a}{v_{act}}$ (4)

Where: Γ = confinement factor, v_{gr} = group velocity, a= differential gain coefficient, V_{act}= active layer volume, N_{tr} = transparency electron number, ε = nonlinear gain coefficient.

β is the spontaneous emission gain and τ_p is the photon lifetime.

The Langevin forces F_N and F_P for electron and photon number fluctuations have been added to account for the laser noise intensity. These functions can be calculated, by the way of their spectral densities and inter-correlation product. For this aim, we adopt the method developed in Reference [3]. The spectral densities are written from the photon and electron rate entering and leaving their own reservoir, and the inter-correlation product is relative to the exchange rates between these reservoirs.

Taking into account the VCSEL specificities, we can write:

$$\left\langle F_N^2 \right\rangle = \frac{\eta_i \cdot I_0}{q} + 2 \cdot N_w \cdot g_0 \cdot \frac{N_{tr}}{1 + \varepsilon \cdot P_0} \cdot P_0 \quad (5)$$

$$\left\langle F_P{}^2 \right\rangle = 2N_w \cdot g_0 \frac{N_{tr}}{1 + \varepsilon P_0} P_0 + 2\frac{P_0}{\tau_p} \quad (6)$$

$$\left\langle F_P \cdot F_N \right\rangle = -\left[2N_w \cdot g_0 \frac{N_{tr}}{1 + \varepsilon \cdot P_0} P_0 + \frac{P_0}{\tau_p} \right] \quad (7)$$

2.2. Behavioral equivalent circuit for different VCSEL structures

With this approach, the physical phenomena occurring in the VCSEL were modeled by an equivalent circuit (Figure 1). We began by adapting the electrical model of edge emitters to the VCSEL. The electronic mechanism in multi QW

active layer is represented by the resistance, R_j ,and the capacitance, C_j. The photon storage and the resonance damping are symbolized by the inductance L_0 and the resistance R_0 respectively.
The current funneling through the DBR is also modeled into our equivalent circuit. For each VCSEL structure, the layer pairs of a DBR are isotype heterojunctions which can be represented by RC parallel elements. All RC circuits in cascade are equivalent to one RC element. For top DBR, we need to take into account the confinement method. In this case (Figure 1), the proton implantation contribution is including into R_{mtop} and C_{mtop}.

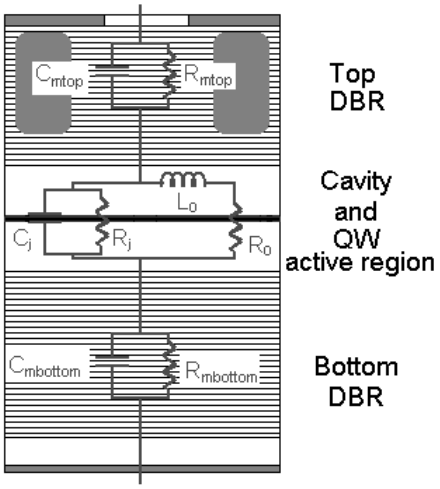

Figure 1. Electrical equivalent circuit of implanted device

For the mesa structure (Figure 2), we have the same cavity and bottom DBR model. The top DBR of the structure shown on Figure 2 a) is crossed by the injection current. This phenomenon is thus represented by the R_{mtop}-C_{mtop} parallel circuit. In the case of the Figure 2 b), the current is directly injected in the cavity. Consequently, the R_{mtop} and C_{mtop} disappear. The contribution of the oxidized region in the cavity can be modeled by the capacitance C_{ox}. In addition, the contact between the anode and the cavity being difficult to realize involves parasitic resistive effects which could be included in the series resistance.

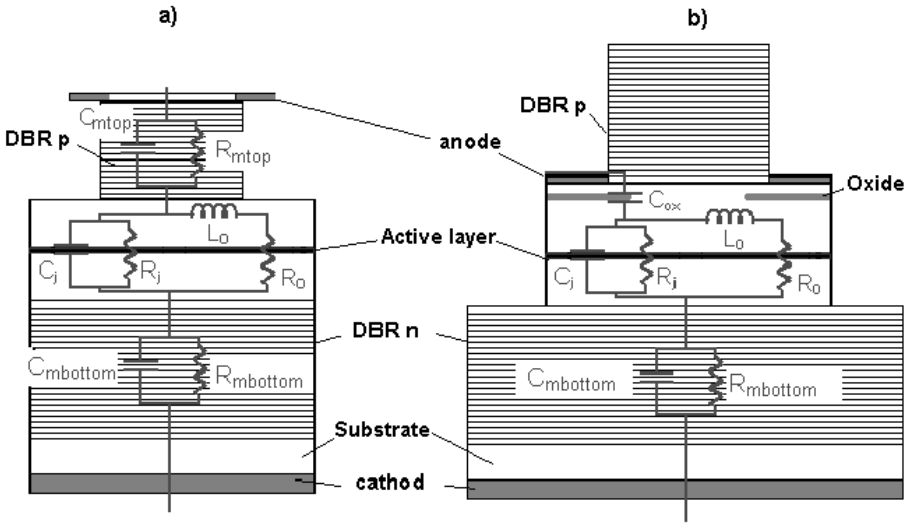

Figure 2: Mesa device a) and intra cavity contacted b)

For the oxide confined VCSEL (Figure 3), we take into account not only the top DBR but also the oxidized region. The variation of the diameter due to the oxide aperture implies resistive and capacitive effects which correspond to R_{ox} and C_{ox} respectively. To simplify the equivalent circuit, we keep only $R_{msup}C_{msup}$ which include R_{ox} C_{ox}.

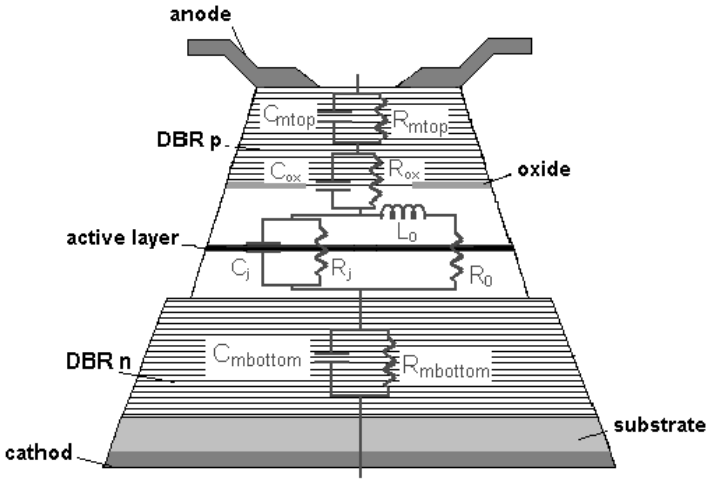

Figure 3:Equivalent circuit of oxide confined VCSEL

This paper presents the test and the modeling of the last VCSEL structure which is designed by Ulm Photonics.

3. EXTRACTION OF INTRINSIC PARAMETERS

3.1. Steady state carrier and photon number

When the steady state is reached, the derivative of carrier and photon number vanishes, then equations (1) and (2) become:

$$0 = N_w \cdot \Gamma \cdot \beta \cdot B \cdot N^2 + N_w \cdot g_0 \cdot \frac{N - N_{tr}}{1 + \varepsilon \cdot P} \cdot P - \frac{P}{\tau_p} \quad (8)$$

$$0 = \frac{\eta_i \cdot I}{q \cdot N_w} - (A + B \cdot N) \cdot N - g_0 \cdot \frac{N - N_{tr}}{1 + \varepsilon \cdot P} \cdot P \quad (9)$$

These two equations can be solved analytically:

- below threshold, by neglected the spontaneous emission and writing P=0.
- above threshold, by considering that the carrier number does not increase above its threshold value N_{th}.

The evolution of the carrier and photon number versus the bias current can be visualized on Figure 4.

For $I=I_{th}$ and $P\cong 0$ the expression of N_{th} is readily derived from (8) to give:

$$N_{th} = \frac{1}{2} \cdot \left(-\frac{A}{B} + \sqrt{\left(\frac{A}{B}\right)^2 + \frac{4 \cdot \eta_i \cdot I_{th}}{B \cdot q \cdot N_w}} \right) \quad (10)$$

P is obtained from equations (7),(8) and (9) as follows:

$$P = \tau_p \cdot \left(N_w \cdot \Gamma \cdot \beta \cdot B \cdot {N_{th}}^2 + N_w \cdot \frac{\eta_i \cdot (I - I_{th})}{q \cdot N_w} \right) \quad (11)$$

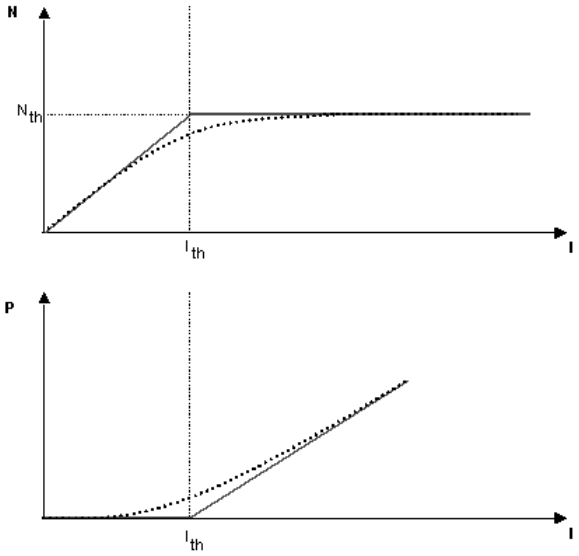

Figure 4: variation of the carrier and photon numbers with the bias current without (solid line) and with the spontaneous emission (dotted line)

3.2. Relationships between intrinsic parameters and elements of the active layer equivalent circuit

Electrical and optical phenomena, described by the rate equations, can be represented by a small signal equivalent circuit as for microwave transistor modeling. The injected current is now a superposition of a bias current I_0 and a small sinusoidal current ΔI(t) such that: $\Delta I(t) << I_o$

Then we can write, on the one hand, the linearized rate equations and, on the other hand, the equations of the active layer equivalent circuit (defined in 2.2).

- Starting from equation (1) and (2) and writing the carrier N and photon P numbers: $N(t) = N_0 + \Delta N(t)$ and $P(t) = P_0 + \Delta P(t)$ with the assumption $\Delta N(t) << N_o$, $\Delta P(t) << P_o$, the linearized rate equations are derived as follows:

$$\frac{d\Delta N}{dt} = \frac{\eta_i}{q \cdot N_w} \cdot \Delta I - \frac{{G_0}^2}{g_0 \cdot (N_0 - N_{tr})} \cdot \Delta P - \left(\frac{G_0}{N_0 - N_{tr}} \cdot P_o + A + 2B \cdot N_0 \right) \cdot \Delta N + F_N \quad (12)$$

$$\frac{d\Delta P}{dt} = N_w \left(\Gamma \cdot 2 \cdot \beta \cdot B \cdot N_0 + \frac{G_0}{N_0 - N_{tr}} \cdot P_o \right) \cdot \Delta N + \left(N_w \cdot \frac{{G_0}^2}{g_0 \cdot (N_0 - N_{tr})} - \gamma_P \right) \cdot \Delta P + F_P \quad (13)$$

- Applying Kirchoff laws in the cavity equivalent circuit (Figure 5a) allows us to derive the differential equations for the sinusoidal current ΔI and voltage ΔV across the junction as:

$$\frac{d\Delta V}{dt} = \frac{\Delta I}{C_j} - \frac{\Delta V}{R_j C_j} - \frac{i}{C_j} \tag{14}$$

$$\frac{di}{dt} = \frac{\Delta V}{L_0} - \frac{R_0}{L_0} i \tag{15}$$

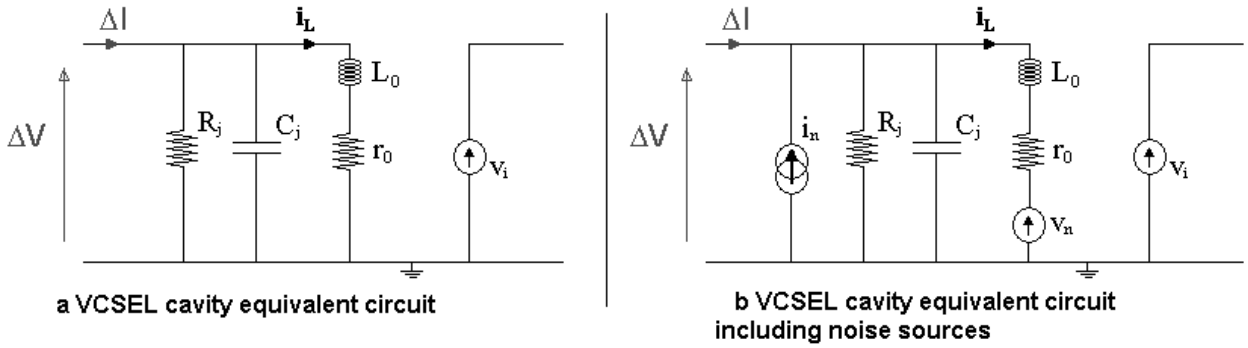

Figure 5:VCSEL cavity equivalent circuit

Using the following relationship:

$$\frac{\Delta V}{V_T} = \frac{\Delta I}{I_0} = \frac{\Delta N}{N_0} \tag{16}$$

(V_T= thermal voltage)

derived from the well-known voltage-current characteristic of a junction, and comparing the two systems of different equations (12)-(13) and (14)-(15), we deduce the expressions of the circuit equivalent elements:

$$C_j = \frac{N_o \cdot q \cdot N_w}{V_T \cdot \eta_i} \tag{17}$$

$$R_j = \frac{V_T}{N_0} \cdot \frac{1}{\left(\frac{I_0 - I_{th}}{N_0 - N_{tr}} + \frac{q \cdot N_w}{\eta_i} \cdot \left(A + 2 \cdot B \cdot N_0 \right) \right)} \tag{18}$$

$$L_0 = \frac{V_T}{N_0} \cdot \frac{q}{\eta_i} \cdot \frac{P_0^{\,2} \cdot g_0 \cdot \left(N_0 - N_{tr} \right)}{\left(I_0 - I_{th} \right)^2} \cdot \frac{1}{\Gamma \cdot 2 \cdot \beta \cdot B \cdot N_0 + \frac{\eta_i}{q \cdot N_w} \cdot \frac{I_0 - I_{th}}{N_0 - N_{tr}}} \tag{19}$$

$$R_0 = L_0 \cdot \left(\gamma_p - \frac{\eta_i^{\,2} \cdot \left(I_0 - I_{th} \right)^2}{q^2 \cdot N_w \cdot P_0^{\,2} \cdot g_0 \cdot \left(N_0 - N_{tr} \right)} \right) \tag{20}$$

From these relations, we can see that C_j, R_j, R_0, L_0 depend on 9 parameters A, B, N_{tr}, τ_P, a, v_{gr}, Γ, β, η_i. A range of each parameter value has been determined from an in-depth literature study (Table 1) [4, 5, 6, 7].

Parameters	Unit	Values
A	s^{-1}	$[1.10^8 ; 1{,}3 .10^8]$
B	s^{-1}	$[0.7 .10^{-16} ; 1.8.10^{-16}] \times V_{act}$
N_{tr}	-	$[0.83. 10^{24} ; 4.4.10^{24}] \times V_{act}$
τ_p	ps	[1; 6]
a	m^2	$[0.2.10^{-20} ; 3.7.10^{-20}]$
v_{gr}	$m.s^{-1}$	$[8.33.10^7 ; 8.6.10^7]$
Γ	-	[0.045 ; 0.06]
β	-	$[10^{-5} ; 10^{-4}]$
η_i	-	[0.6 ; 0.86]

Table 1: intrinsic parameters range of 850nm VCSEL

Initial values of all these parameters are selected from that table to be used as the starting point of the optimization process which yields the equivalent circuit elements of the VCSEL (see part 4).

3.3. Spectral densities of voltage and current noise sources

According to the analogy between rate equations and equivalent electrical circuit, the Langevin forces can be identified as electrical noise sources as shown in Figure 5.b. This representation is independent of the DBR structure type.
The equations describing the equivalent circuit including noise sources are written as follows:

$$\frac{d\Delta V}{dt} = -\frac{\Delta V}{R_j C_j} - \frac{i_L}{C_j} + \frac{\Delta I}{C_j} + \frac{i_n}{C_j} \qquad (21)$$

$$\frac{di_L}{dt} = \frac{\Delta V}{L_0} - \frac{r_0}{L_0} \cdot i_L - \frac{v_n}{L_0} \qquad (22)$$

Through the transformation used in §3.2, the spectral densities of the noise sources and their intercorrelation function are derived as:

$$S_{ii} \triangleq \frac{\overline{i_n^2}}{\Delta f} = 2\frac{q^2}{\eta_i^2} < F_N^2 > \qquad (23)$$

$$S_{vv} \triangleq \frac{\overline{v_n^{\,2}}}{\Delta f} = \frac{V_T^{\,2}}{\left(2 \cdot \Gamma \cdot \beta \cdot B \cdot N_0 + g_0 \frac{P_0}{1+\varepsilon \cdot P_0}\right)^2 N_0^{\,2} N_w^{\,2}} < F_P^{\,2} > \qquad (24)$$

$$S_{iv} \triangleq \frac{\overline{i_n \cdot v_n}}{\Delta f} = \frac{q}{\eta_i} \frac{V_T}{\left(2 \cdot \Gamma \cdot \beta \cdot B \cdot N_0 + g_0 \frac{P_0}{1+\varepsilon P_0}\right) N_0 N_w} < F_P F_N > \quad (25)$$

4. S PARAMETERS SIMULATION AND MEASUREMENT

Values of small-signal equivalent circuit elements have been obtained from the measurement of the S11 and S21 parameters. The measurements are realized with the experimental setup illustrated in the Figure 6.
The VCSEL is modulated through a probe connected to a vectorial network analyzer. The emitted light is picked up by an optical fiber which is connected to a photoreceiver. The amplified photodetected signal is then measured at port 2 of the network analyzer.

The measured S11 and S21 of the whole optoelectronic link were implemented in a CAD software to fit their counterparts calculated from the sinusoidal signal equivalent circuit (Figure 7).
After de-embedding, the S-parameters of the VCSEL were obtained for several bias currents and in the frequency range [45MHz-10GHz].

Results for 20µm aperture size VCSEL and 10mA bias current are shown in Figure 8 and 9. The agreement between measured and simulated scattering parameters is quite good and allows us to extract confident values of chip parameters.

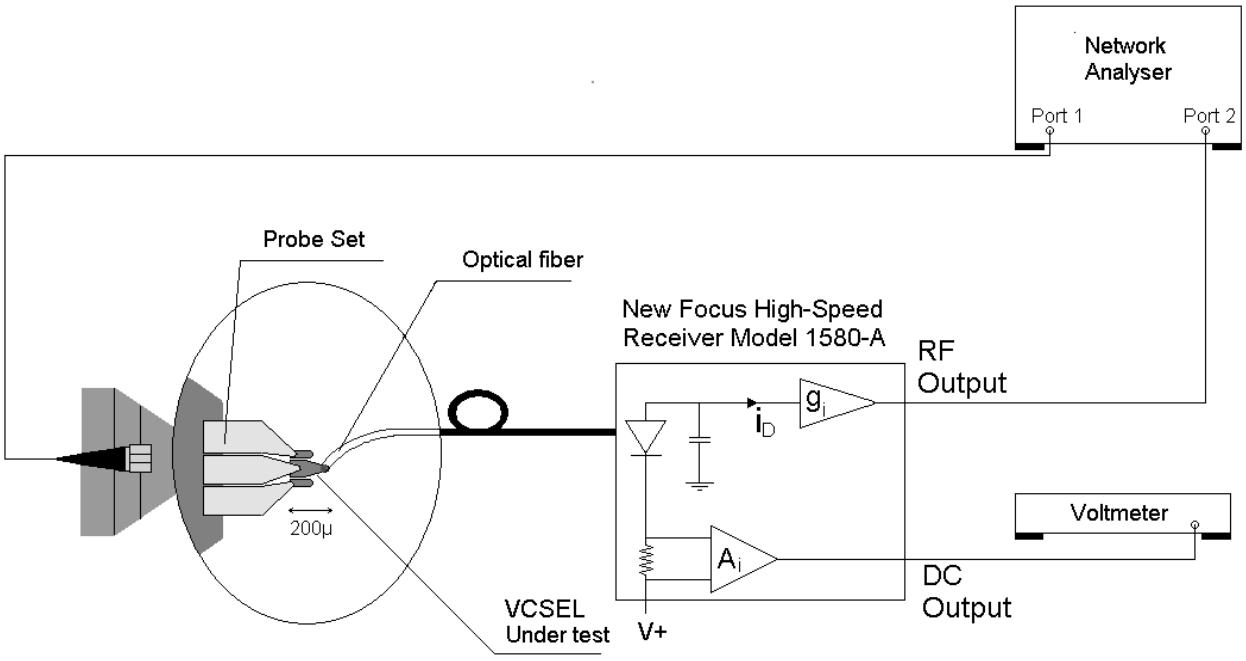

Figure 6: experimental arrangement for S11 and S21 parameters measurement

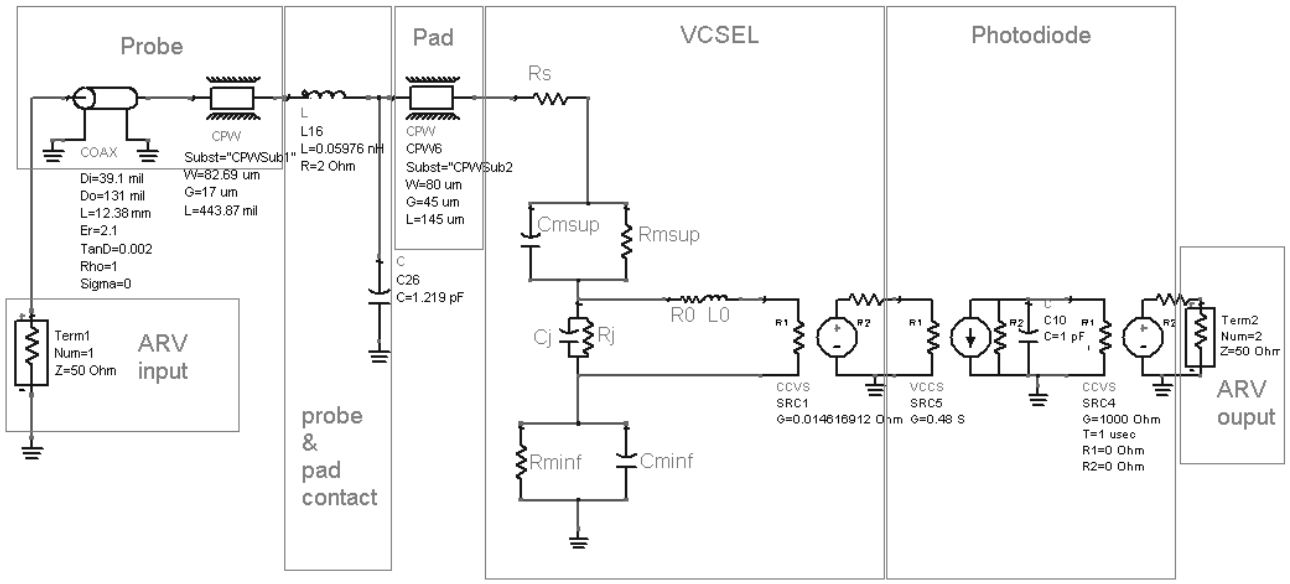

Figure 7: small signal equivalent circuit of the complete link

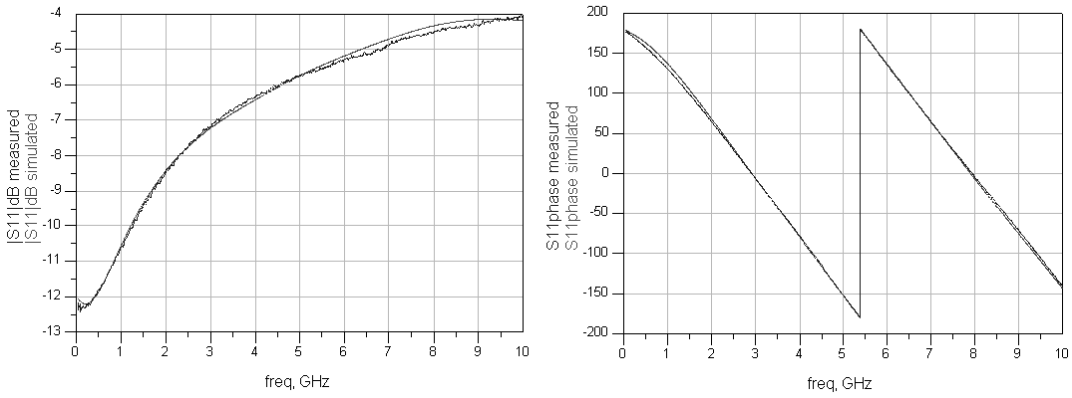

Figure 8: comparison between simulated and measured S11 module (left curve) and phase (right curve)

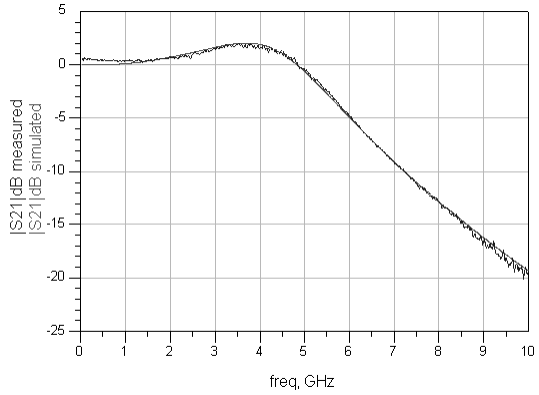

Figure 9: comparison between simulated and measured S21 module

Different VCSEL with aperture size ranging between 10 to 25µm were tested and the parameters values are given on the following table.

∅ (µm)	I (mA)	Rj (ohm)	Cj (pF)	Ro (ohm)	Lo (pH)	Rs (ohm)	Rmtop (ohm)	Cmtop (pF)	Rmbottom (ohm)	Cmbottom (pF)
25	20	2,24	97	0,18	9,4	10,55	7,9	7,77	2,18	101
	10	3,76	97	0,19	21,50	7,5	11,39	4,285	1,4	101
20	10	3,93	86,76	0,24	14,87	12,522	14,92	4,35	1,37	101
14	10	4,30	70,20	0,26	8,08	25,13	13,38	4,263	4,52	101
	5	4,42	70,20	0,30	16,74	31,18	14,11	2,93	4	101
12	5	4,76	70,13	0,29	12,86	29,14	20,8	3	4,96	101
	2	5,09	70,13	0,319	41,35	31,12	33,86	2,236	13,45	101
10	5	5	70	0,29	9,34	23,4	36	1,43	5,1	101
	2	5,2	70	0,38	26	32,01	47,8	12,6	1,39	101

Table 2: VCSEL equivalent circuit elements values

It may be verified according to the relations (17) to (20) that:

- R_j decreases and C_j increases when the aperture size and the bias current increase.
- R_0 decreases and L_0 increases when the bias current decreases and the aperture size increases

From the knowledge of the VCSEL electric equivalent circuit, the 9 intrinsic parameters (given on Table 1) were extracted by optimization. Finally, from equations (10) and (11), some physical parameters like carrier and photon numbers were derived. Typical values were found as: $N=1.1*10^7$, $P=3.38*10^5$.

From the measurement of VCSEL scattering parameters, we are then able to extract several intrinsic parameters of this device with a minimum of manufacturer data.

5. RELATIVE INTENSITY NOISE MEASUREMENT AND COMPARISON

Relative Intensity Noise measurements have been realized for various oxide aperture diameters and bias values.
The experimental setup placed in a Faraday cage was similar to the test bench used for S-parameters measurements except for two components (Figure 10):

- A controlled bias source is connected to the probe tester.
- The photoreceiver was connected to a Rhode&Schwarz spectrum analyzer.

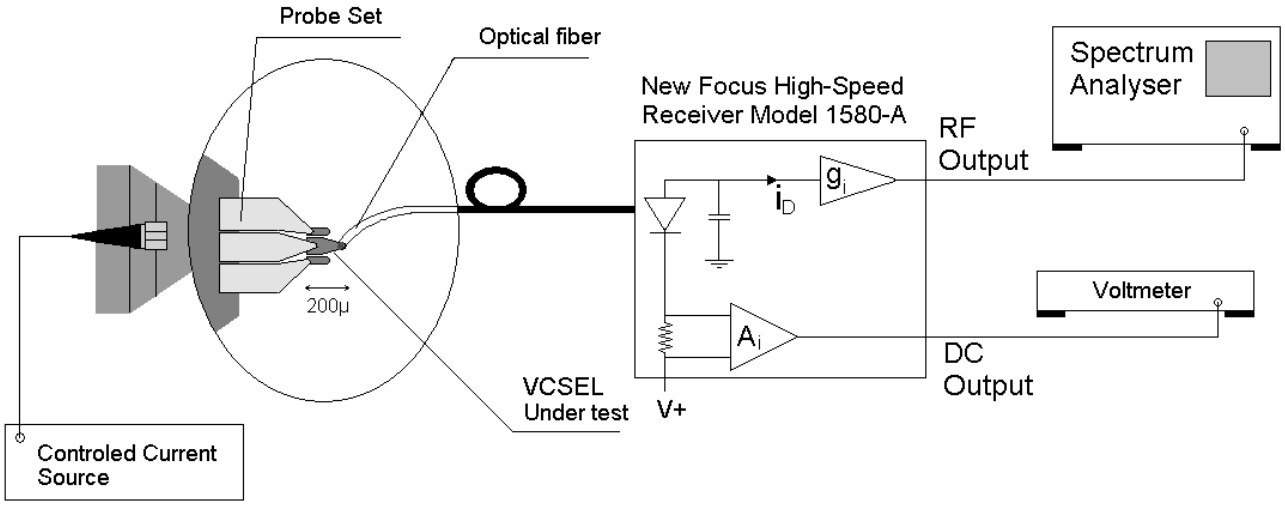

Figure 10: experimental arrangement for RIN measurement

Two steps are needed to obtain the experimental RIN. First, an acquisition without laser emission is done, which allows a good estimation for the link noise including the photodiode dark noise, the amplifier thermal noise and the noise of the spectrum analyzer. Second, the VCSEL is biased and the data are collected and processed to extract the laser intensity noise. Figure 11.a shows results for a 12µm aperture size Ulm Photonics VCSEL for various bias current from $I_{threshold}$ up to $2.5I_{threshold}$ and frequencies ranging from 45MHz to 8GHz.

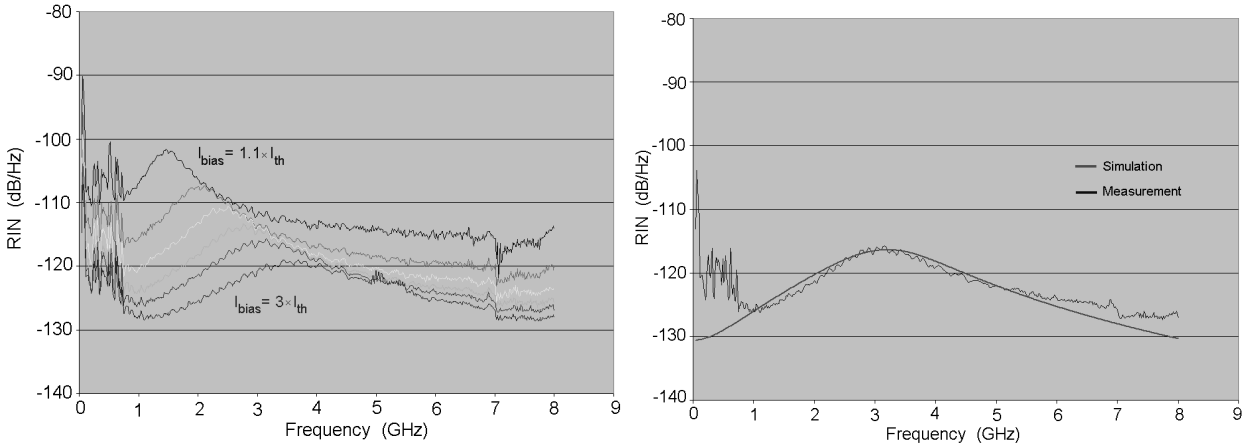

a: RIN measurements for various bias currents

b: RIN simulation for $I_{bias}= 2I_{threshold}$

Figure 11:Measurements and simulation for a 12µm aperture ULM VCSEL

The global electrical model including Bragg reflectors and active area taking noise into account is then built and optimized with the ADS™ simulator. The resistive, capacitive and inductive elements which are already extracted from the S-parameters measurements are not involved in the optimization process. An easy manual optimization on the noise sources amplitude allows to fit the curves as shown in Figure 11.b. We note a fairly good agreement between simulation and measurement except at low frequencies. The origin of this noise excess is not well understood at present.

6. CONCLUSION

We have made a complete equivalent electrical model of various VCSEL structures. The signal modeling demonstrate a good capacity to extract the physical parameters of the device and it allows predictions of the dynamic VCSEL behavior for bias current variations. The noise modeling is very efficient to determine the RIN characteristics of the emitter. Moreover, this model can be readily inserted into the electrical environment of the laser diode and it could become a master piece for modeling any optomicrowave link. For this objective further studies on the low noise behavior have to be realized.

7. ACKNOLEDGMENTS

We would like to grateful acknowledge Ulm Photonics for providing the VCSEL arrays. We also acknowledge M. PEZ from D-Lightsys for his collaboration.

8. REFERENCES

[1] A. Rissons, J-C Mollier, Z. Toffano, A. Destrez, M. Pez, *"Thermal and Optoelectronic Model of VCSEL Arrays for Short Range Communications", VCSEL VII,* SPIE Proceeding 4994, paper n° 4994-13, January 2003.

[2] A. Rissons, J. Perchoux, J-C.Mollier, "*Small Signal And Noise Circuit Model Of Vertical-Cavity Surface-Emitting Laser (Vcsel) Arrays For Short Range Optomicrowave Links",* Microwave Photonics 2003, Budapest (Hungry), September 2003.

[3] Christoph Harder, Joseph Katz, S. Margalit, J. Shacham, and Amnon Yariv, "Noise Equivalent Circuit of a Semiconductor Laser Diode", IEEE Journal of Electronics, Vol. QE-18, No. 3, March 1982.

[4] Matt Bruensteiner et George C. Papen, *" Extraction of VCSEL Rate-Equation Parameters for Low-Bias System Simulation"* , IEEE JOURNAL OF SELECTED TOPICS IN QUANTUM ELECTRONICS , Vol.5, No.3, pp.487-493, Mai/ Juin 1999.

[5] X. Li, T.E. SALE, G. Knowles, *"Integrated Optical Electronic Modelling of Oxide Confined Visible VCSEL" ,* Vertical-Cavity Surface-Emitting Laser VI, SPIE Proceeding, Vol. 4649, Janvier 2002

[6] L.A. Coldren, S.W. Corzine, *"Diode Lasers and Photonic Integrated Circuits",* John Wiley & Sons, 1995

[7] Hi. Li , K. Iga, *"Vertical-Cavity Surface-Emitting Laser Devices*", Springer, 2002.